Formation of β"-related composite precipitates in relation to enhanced thermal stability of Sc-alloyed Al-Mg-Si alloys

Y. Liu[a], Y.X. Lai[a,*], Z.Q. Chen[a], S.L. Chen[b], P. Gao[b], J.H. Chen[a,*]

[a] Center for High-Resolution Electron Microscopy, College of Materials Science & Engineering, Hunan University, Changsha, Hunan 410082, China
[b] Electron Microscopy Laboratory and International Center for Quantum Materials, School of Physics, Peking University, Beijing 100871, China

ARTICLE INFO

ABSTRACT

The Al-Mg-Si alloys added with trace Sc demonstrates an improved thermal stability, as compared with that without Sc-addition. But the microstructural origin of the enhanced property is unclear. In the present study, the precipitates formed in an Al-Mg-Si-Sc alloy were studied in detail by atomic-resolution scanning transmission electron microscopy. It is shown that the dominant precipitates formed at the peak-aging condition are the disordered β" precipitates consisting of Sc-free β" sub-units and Sc-containing disordered regions, rather than the well-ordered β". Upon further aging, these disordered β" precipitates will evolve to β"/β'/B′/U2 composite precipitates. The formation of the composite precipitates is probably associated with the strong binding between Sc and Si atoms, and with the non-preference for Sc atoms to occupy the atomic sites of the β"-structure. Our study reveals the following: It is the formation of stabilized β"-related composite precipitates that enhances the thermal stability of the Sc-added Al-Mg-Si alloy.

1. Introduction

The heat-treatable Al-Mg-Si alloys (known as 6xxx series) have been widely used in automobile and aviation industries due to their good formability, high strength-to-weight ratio, and low cost [1]. Nano-sized metastable precipitates formed in the Al-matrix with different crystal structures, sizes, number densities and volume fractions have a direct impact on the mechanical properties of Al alloys. The precipitation sequence of Al-Mg-Si alloys is commonly described as [2,3]: supersaturated solid solution (SSSS) → atomic clusters → GP zones → β" → β' (/B′/U1/U2) → β. The needle-like monoclinic β" phase, mostly formed at the peak-aging condition, is regarded as the most effective hardening precipitate in Al-Mg-Si alloys [4–6]. Its composition is normally accepted as Mg_5Si_6 [3,4], while recent studies suggest that its energetically favorable composition is $Mg_{5-x}Si_4Al_{2+x}$ (0 ≤ x ≤ 1) [7,8]. The rod-like/lath-like β' (hexagonal Mg_9Si_5), B′ (hexagonal $Al_3Mg_9Si_8$), U2 (orthorhombic $Mg_2Al_2Si_2$), and U1 are generally formed in over-aged conditions and responsible for softening of the alloys [9–14]. For convenience in understanding the structure analysis in the present work, Fig. 1 gives schematically the atomic-structure models of encountered known

phases in Al-Mg-Si alloys. Note that the structure portion(s) indicated by green circle, pink triangle, orange triangles, and blue hexagons are the characteristic sub-unit(s) of β", β', B′, and U2 respectively. The sub-unit of β" was referred to as a "low-density cylinder" (LDC) in the literature [15]. Nevertheless, our recent studies have demonstrated that the precipitation sequence of Al-Mg-Si alloys is actually closely associated with alloy composition, thermo-mechanical process applied, and addition of micro-alloying elements [16–19].

Improving the mechanical properties of Al-Mg-Si alloys by adding alloying elements has long been serious issue in developing advanced automotive aluminum materials [20–23]. As a typical example of micro-alloying elements for Al alloys, Sc has been reported to be the most effective strengthening element per atomic fraction in the Al-matrix [24,25], though addition of Sc is unlikely to be realistic. Among the studies on the Sc micro-alloying in Al alloys, although early studies were mainly.

focused on the advantages of removing impurities and refining grains induced by the Sc addition [26–28], the Sc effect on precipitation has been attracting more and more interest. On the one hand, Sc is utilized to micro-alloy pure Al or other non-heat-treatable Al alloys (e.g., Al-Mg and Al-Si alloys) to make them heat-treatable by forming nanosized Al_3Sc precipitates [29,30]. On the other hand, there have been extensive studies on the Sc micro-alloying in heat-treatable Al alloys. Since the aging temperature of common heat-treatable Al alloys is too low to form Al_3Sc

---

* Corresponding authors.
  E-mail addresses: lyxzhc123@hnu.edu.cn (Y.X. Lai), jhchen123@hnu.edu.cn (J.H. Chen).
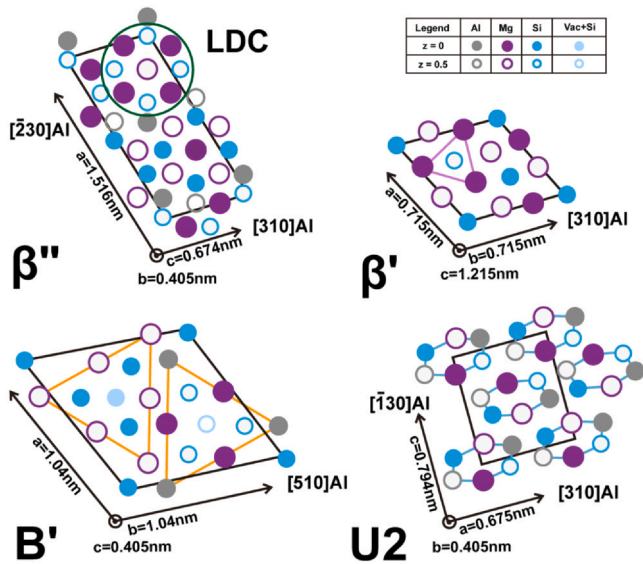
Fig. 1. Schematic drawing of the unit cell of β″, β′, B′, and U2. The characteristic sub-unit(s) of the four phases are marked by green circle, pink triangle, orange triangles and blue hexagons, respectively.

precipitates [31], the Sc micro-alloying in heat-treatable Al alloys is mainly to affect their intrinsic precipitation behavior and consequently their properties [27,32–38]. For instance, it has been demonstrated by atom probe tomography that the Sc atoms are prone to segregate at the θ′/matrix interfaces in an Al-2.5Cu-0.3Sc alloy (wt %), which refines the distribution of θ′ precipitates and hence enhances the strengthening response [32]. It has also been shown for an Al-Cu-Mg-Ag alloy with 0.32 wt% Sc addition that Sc could retard the nucleation of Ω phase, which results in degraded age-hardening capacity and strength properties of the alloy [33].

However, the effects of Sc addition on the age hardening of Al-Mg-Si alloys remain controversial [27,34–38]. It was reported that a combined addition of Sc and Zr results in a reduction of peak hardness but in an improvement of thermal stability during aging at 190 °C in an AA6061 alloy [27]. While another group used the unique impact of precipitate coherency on resistivity and hardness to establish the Al-Mg-Si(-Sc-Zr) precipitation sequence during isochronal aging, and found that the addition of Sc and Zr has no visible effect on the aging behavior of the Al-Mg-Si alloy [34]. Unfortunately, there was a lack of detailed characterization of the precipitate microstructures of Sc-containing Al-Mg-Si alloys in previous studies, making the role of Sc in the precipitation of the alloys poorly understood. Understanding of this issue will not only clarify the effects of Sc addition on the age hardening of Al-Mg-Si alloys, but also be expected to provide insight into micro-alloying strategy for the alloys. According to the latest extensive first-principles calculation based database [39], the binding energy of Sc-vacancy and that of Sc-Si are much higher than that of Sc-Mg, implying that Sc has great potential to influence the precipitation behavior of Al-Mg-Si alloys.

In the present work, atomic-resolution high-angle annular dark-field scanning transmission electron microscopy (HAADF-STEM) and first-principles calculations were employed to characterize the precipitate microstructures of a Mg-excess Sc-containing Al-Mg-Si alloy. We demonstrate that this alloy has distinctly different precipitate microstructures compared with the Sc-free counterpart, in which disordered β″ precipitates composed of Sc-free β″ sub-units and Sc-containing disordered regions form firstly. Upon over-aging, the disordered β″ precipitates then evolve to fine composite precipitates containing β″ sub-units instead of the coarse β′ precipitates. Our

study reveals the microstructural origin of the trace-Sc-enhanced thermal stability of Al-Mg-Si-Sc alloys.

2. Experimental and computational procedures

Two alloys with chemical compositions of Al-1.4Mg-0.5Si (wt%) and Al-1.4Mg-0.5Si-0.2Sc (wt%) were used in this study. The as-cast alloys were homogenized at 500 °C for 10 h, and hot- and cold-rolled to 1 mm thick sheets. After that, these sheets were solution heat treated at 565 °C for 0.5 h, water quenched to room temperature, and immediately aged in an oil bath at 180 °C for different times. Vickers hardness was measured with a load of 4.9 N and a dwell time of 10 s, and the hardness values were the average values of at least 5 indentations. Transmission electron microscopy (TEM) and high-resolution TEM (HRTEM) observations were carried out with a FEI Tecnai F20 TEM operated at 200 KV. HAADF-STEM imaging was performed using an aberration-corrected FEI Titan Cubed Themis G2 operated at 300 KV. All microstructure images were taken along a < 100 >$_{Al}$ zone axis. To reduce noise, all the HAADF-STEM images were Fourier filtered with an aperture encompassing all the visible spots in the Fourier transform. The TEM/STEM specimens were prepared by electro-polishing using a Tenupol 5 machine (Struers) with an electrolyte of 1/3 HNO$_3$ in methanol at a temperature below −25 °C. In order to reduce the effect of contamination, all specimens were cleaned before HAADF-STEM observation using a Model 950 plasma cleaner (Gatan).

Density functional theory (DFT) calculations in the present work were carried out using the Vienna Ab initio Simulation Package (VASP) [40–43] with projector-augmented wave (PAW) potential [44,45]. The generalized gradient approximation (GGA) with the exchange-correlation function of Perdewe-Burkee-Ernzerhof (PBE) [46] was employed. Plane wave cutoff energy was set to be 350 eV in all the calculations. K-points sampling was carefully selected to ensure convergence in the order of a few meV atom^{-1}. The formation enthalpy of precipitate structures was calculated according to Ref. [15]. The formation enthalpy of an Al$_x$Mg$_y$Si$_z$Sc$_m$ phase with respect to the solid solution is determined by the following equation:

$$\Delta H_{ss}^{form}(Al_xMg_ySi_zSc_m) = H(Al_xMg_ySi_zSc_m) - xH(Al^{fcc})$$
$$- yH(Mg^{sub}) - zH(Si^{sub}) - mH(Sc^{sub}) \quad (1)$$

where x, y, z and m are the atomic fractions (x + y + z + m = 1). H (Al$_x$Mg$_y$Si$_z$Sc$_m$) is the total energy of Al$_x$Mg$_y$Si$_z$Sc$_m$ phase per atom. H (Mg^{sub}), H(Si^{sub}) and H(Sc^{sub}) are the enthalpies of Mg, Si and Sc atoms on substitutional sites in the Al-matrix, respectively. The enthalpy H(Mg^{sub}) is calculated in a supercell containing 108 atoms (based on 3 × 3 × 3 unit cells of Al) with the formula as:

$$H(Mg^{sub}) = H(Al_{107}Mg) - \frac{107}{108}H(Al_{108}) \quad (2)$$

An analogous formula is valid for H(Si^{sub}) and H(Sc^{sub}).

3. Results and discussion

3.1. Age-hardening responses

Fig. 2 shows the age-hardening responses of the Sc-free and Sc-containing alloys aged at 180 °C, where Vickers hardness is presented as a function of aging time. The hardness of the two alloys firstly increases rapidly with prolonged aging time until it reaches the peak-aged status after 8 h. The Sc-containing alloy possesses a lower peak hardness than the Sc-free alloy. Upon further aging, the hardness of the Sc-free alloy decreases gradually. In contrast, for the Sc-containing alloy, the hardness maintains the same level as its peak hardness even after extended aging of up to 40 h, and
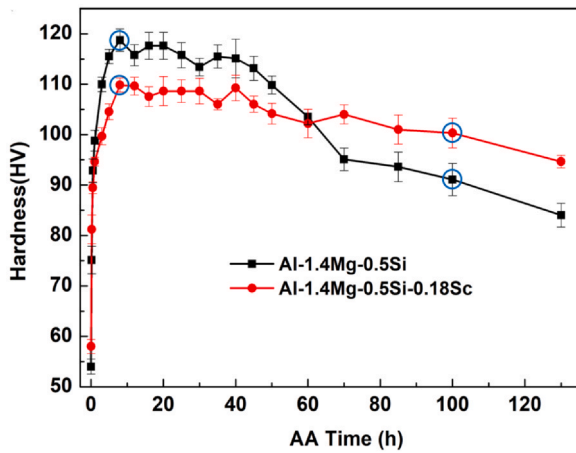
Fig. 2. Age-hardening curves of the two investigated alloys aged at 180 °C for different times.

subsequently decreases at a much slower rate compared with the Sc-free alloy upon aging up to 100 h. Obviously, Sc addition generates a decrease in peak-aged hardness and an improvement in thermal stability, which is consistent with the results reported in [27]. Four samples marked with blue circles in Fig. 2 were selected for TEM and HRTEM observations.

3.2. TEM/HRTEM overviews of typical precipitate microstructures

Low-magnification TEM images and the corresponding typical HRTEM images of the precipitates formed in the two alloys under two aging conditions are presented in Fig. 3. The precipitate length distributions measured on the same samples in Fig. 3 are shown in Fig. 4. For each aging condition, at least three TEM images were selected and the amount of precipitates taken into account was more than 200 to ensure the accuracy of measurement. For the Sc-free alloy, the precipitates in both the peak-aging and over-aging conditions are uniformly dispersed in the matrix. The precipitates in the 100 h over-aging condition have an average length of 111 nm, which are significantly coarser than the ones in the peak-aging condition with an average length of 8 nm (Fig. 3a and c, Fig. 4a and b). As proved by the HRTEM images and the inserted fast Fourier-

transform (FFT) patterns shown in Fig. 3(b) and (d), the primary precipitates of the peak-aged and over-aged samples are the needle-like β" and rod-like β' precipitates, respectively. The above observations agree well with previous studies [18]. In contrast, the Sc-containing alloy exhibits distinctly different precipitate micro-structures. At the peak-aging state, fine needle-like precipitates and relatively coarse rod-like precipitates both form in the matrix, yielding an average precipitate length of 34 nm (Fig. 4c). Additionally, the proportion of the needle-like precipitates is evidently higher than that of the rod-like ones (Fig. 3e). At the 100 h over-aging state, the precipitate morphologies (i.e., needle and rod) and the frequencies of precipitates in the two morphologies are basically unchanged but the overall precipitate size is slightly increased compared with those at the peak-aging state (Figs. 3g and 4d). Representative HRTEM images of the fine needle-like precipitates dominated in Fig. 3(e) and (g) are shown in Fig. 3(f) and (h), respectively. It is clear that these precipitates have no recognizable periodic features and are hardly to be identified. As for the rod-like precipitates, their lattice structures revealed by HRTEM are the same as β'. Worth mentioning is that no Al_3Sc nanoprecipitates are observed in the Sc-containing alloy, because the aging temperature of 180 °C is lower than the ordinary formation temperature (250–500 °C) of Al_3Sc [31].

The TEM and HRTEM observations have indicated that Sc addition changes not only the precipitate size but also the precipitate crystalline type. At the peak-aged state, all precipitates in the Sc-free alloy are the β" precipitates, while the precipitates in the Sc-containing alloy are mostly disordered precipitates and partially the β' precipitates. At over-aged stage, the coarse β' precipitates constitute the main precipitates in the Sc-free alloy, while there exist a large number of relatively fine disordered precipitates in the Sc-containing alloy. The above observed microstructural variations have provided useful information for understanding the changes in age-hardening response demonstrated in Fig. 2. However, to fully understand the Sc micro-alloying, atomic-structures of the disordered precipitates formed in the Sc-containing alloy have to be revealed.

3.3. Atomic-structures of the precipitates in the Sc-containing alloy

Atomic-resolution HAADF-STEM imaging was employed to characterize the precipitates of the Sc-containing alloy under the
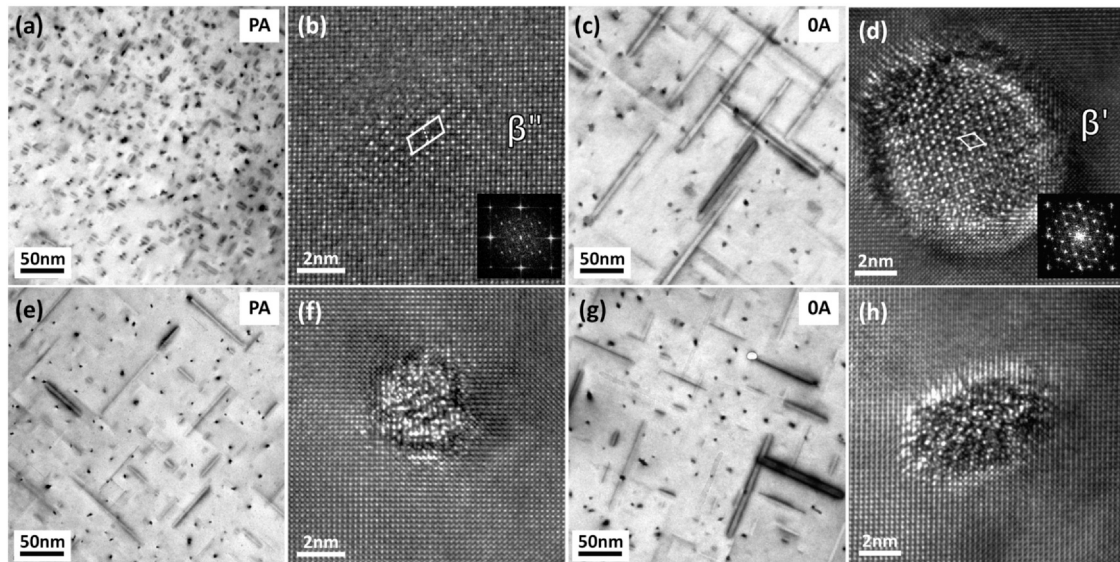
Fig. 3. TEM bright-field images and the corresponding HRTEM images of the typical precipitates in the two alloys aged at 180 °C for different times. (a–d) Sc-free alloy, (e-h) Sc-containing alloy; (a, b, e, and f) 8 h peak-aging, (c, d, g, and h) 100 h over-aging.
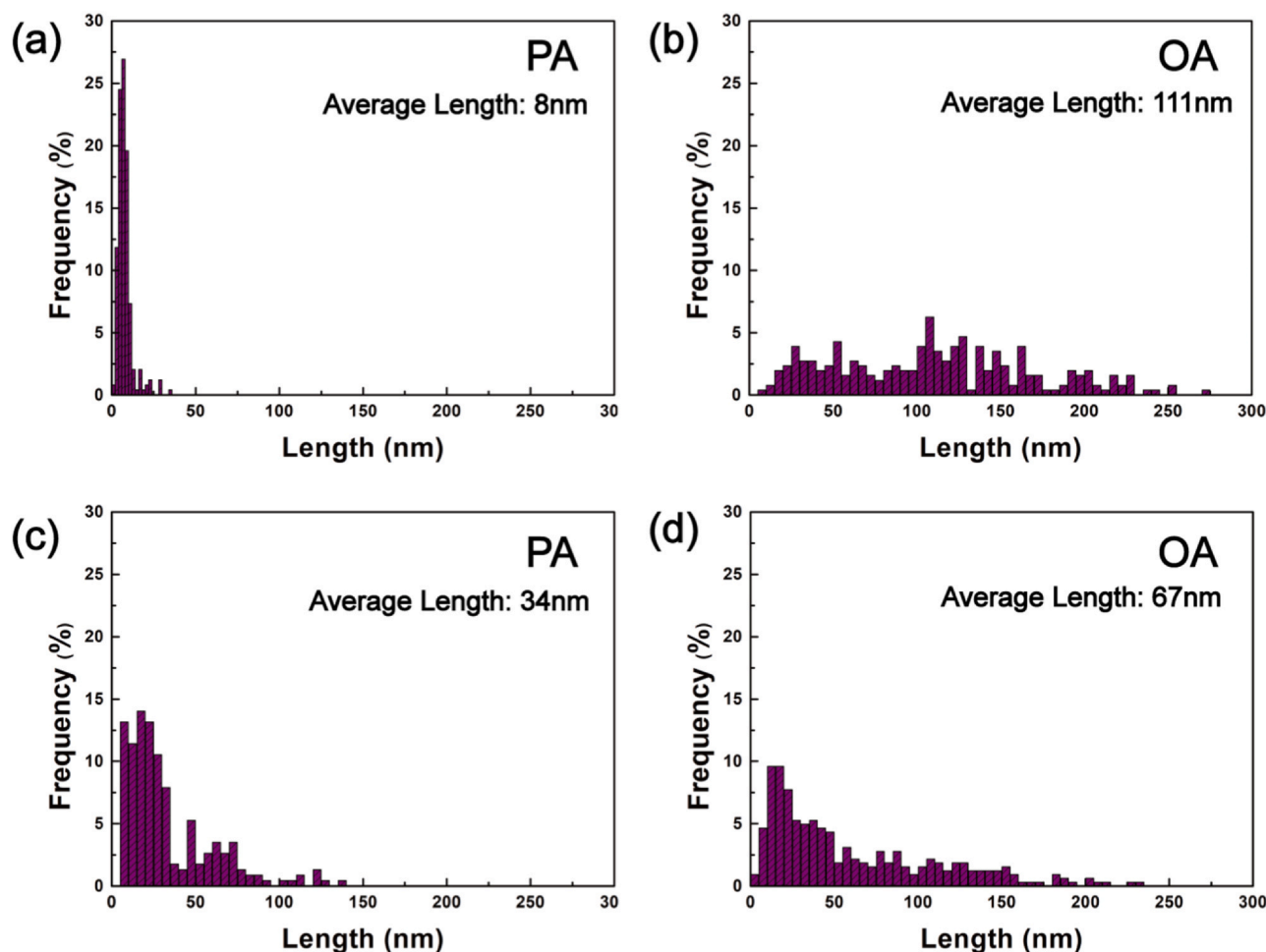
Fig. 4. Precipitate length distributions for the two alloys aged at 180 °C for different times. (a, b) Sc-free alloy, (c, d) Sc-containing alloy; (a, c) 8 h peak-aging, (b, d) 100 h over-aging.

peak-aging and over-aging conditions. The obtained images show Z-contrast (where Z represents the atomic number of the atom) proportional to $Z^{1.7-2.0}$ [47]. In this study, Sc columns appear as the brightest dots as Sc has a much higher atomic number (Z = 21) than the other three elements (Z = 14 for Si, 13 for Al, and 12 for Mg). Consistent with the TEM findings (Fig. 3e–h), the structures of precipitates at the two aging states can be roughly divided into two types, and their typical images are shown in Figs. 5 and 6. Fig. 5(a) and (b) show two examples of the dominant needle-like precipitates at peak-aging. The LDCs are clearly observed in the precipitates. It is interesting that apart from the LDCs, these precipitates also contain disordered regions where atoms arrange in a quite random manner. Occasionally, one sub-unit of β' or B′ is present in the disordered regions, as shown in Fig. 5(a) and (b). In the following we refer to these precipitates as disordered β" precipitates. The atomic column Z-contrast indicates that there are no Sc atoms in the LDCs, while Sc atoms are incorporated in a few columns in the disordered regions. In particular, in Fig. 5(a) and (b), the Sc atoms are situated in the column that belongs to the sub-unit of β' or B′. Another precipitate type present at peak-aging is the β' phase, whose typical image is shown in Fig. 6(a).

For the 100 h over-aging condition, precipitates with complex structures were frequently observed, as shown in Fig. 5(c) and (d). These precipitates feature predominantly sub-units of late-stage β'/B′/U2, as well as several LDCs. They are referred to as composite precipitates. The β' precipitates were also observed here, as shown in Fig. 6(b). Quantitative statistics of the precipitates show that the

composite precipitates account for nearly 80% of the precipitates. Comparing the precipitate structures under the two aging conditions, it is easy to judge that the composite precipitates and β' at over-aging should be evolved from the disordered β" and β' at peak-aging, respectively. The disordered β" precipitates and composite precipitates without even one complete unit cell correspond to the disordered precipitates observed in the HRTEM images (Fig. 3f and h).

The transformation from disordered β" to composite precipitates generates not only more ordered precipitate structures, but also a higher degree of Sc incorporation in the precipitate structures. Line profile analyses of the atomic column intensities in Fig. 5(c) and (d) reveal the partial Sc occupation at specific featured atomic sites of β' and B′ structures. Some of the Mg-site columns in β' (e.g. b of Profile 1 in Fig. 5c) and some of the Mg1/Mg3-site columns in B′ (e.g. b of Profile 2 in Fig. 5c) are brighter than the normal Mg columns, indicating that these Mg-site columns contain Sc atoms. In addition, some of the Mg2/Al-site columns in B′ (e.g. b and c of Profile 3 in Fig. 5(c), and a and c of Profile 3′ in Fig. 5d) are also observed to contain Sc atoms. When the sub-B′ is located at the precipitate/matrix interface, Sc occupation at the central site of sub-B′ (e.g. the sub-B′ in the upper left corner of Fig. 5d) is occasionally observed. Note that the sub-B′ with central Sc in Fig. 5(b) also happens to be located at the precipitate interface. The statistics from nearly 10 composite precipitates in total consistently support the above observations. Another common feature of the precipitates at over-aging is the Sc segregation at the precipitate/matrix interfaces, as
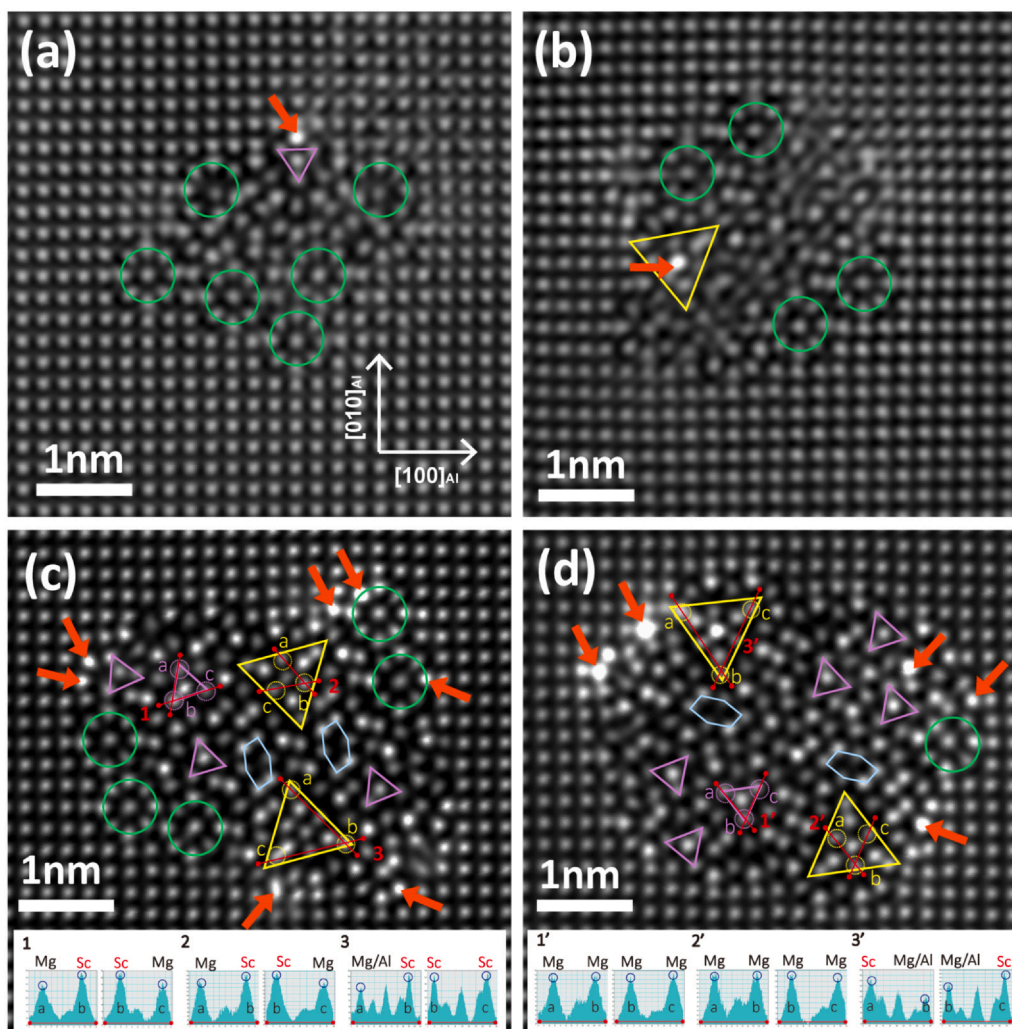
Fig. 5. Atomic-resolution HAADF-STEM images of typical precipitates formed in the Sc-containing alloy aged at 180 °C for different times. (a, b) Disordered β″ precipitates at 8 h peak-aging, (c, d) β″/β′/B′/U2 composite precipitates at 100 h over-aging. The red arrows indicate the distinct Sc atomic columns. The three red open circles, marked as a, b, and c, located in each phase sub-unit in (c) and (d) indicate three equivalent atomic columns. The intensity line profiles (named as 1, 2, 3 in (c), and 1′, 2′, 3′ in (d)) between these columns are shown as insets in the bottom parts.
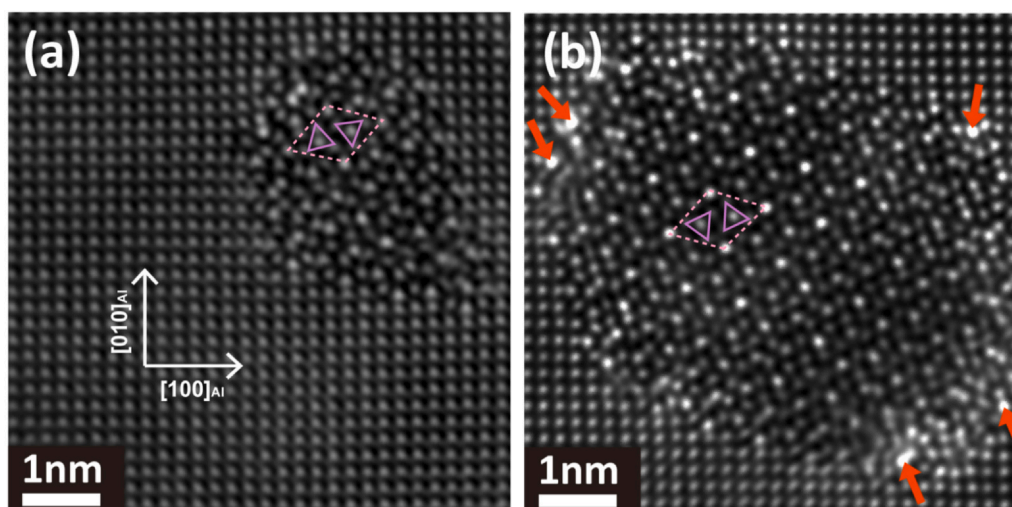
Fig. 6. Atomic-resolution HAADF-STEM images of β′ precipitates formed in the Sc-containing alloy aged at 180 °C for different times. (a) 8 h peak-aging, (b) 100 h over-aging. The red arrows in (b) indicate the distinct Sc atomic columns.
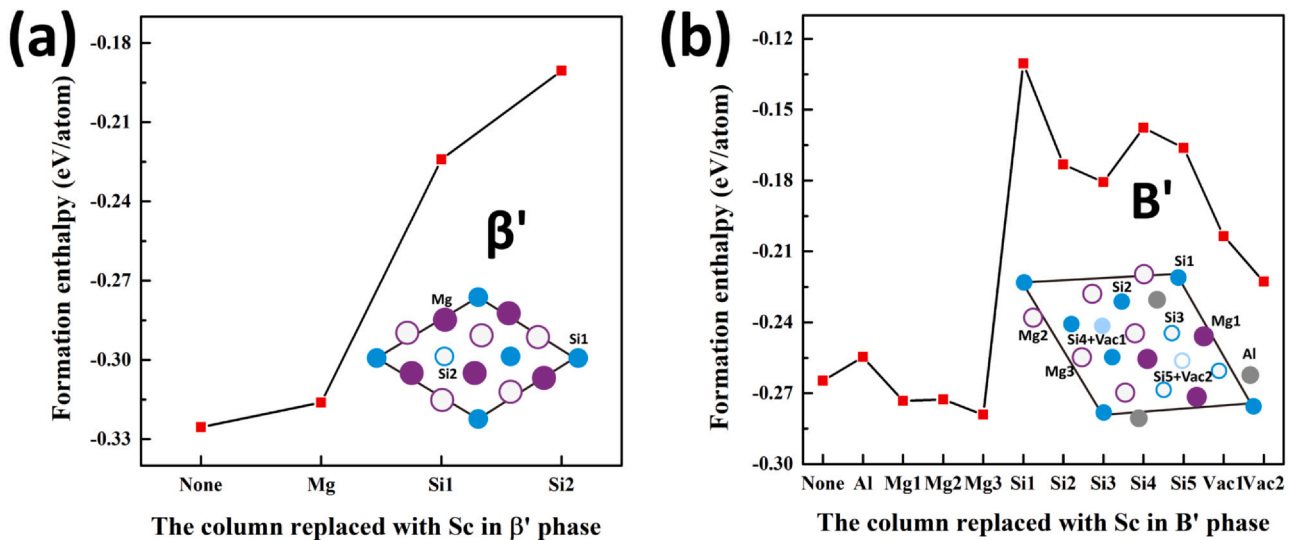
Fig. 7. The formation energy per atom of β′ (a) and B′ (b) with different atomic columns substituted by Sc.

indicated by the red arrows in Figs. 5(c) and (d) and 6(b). A similar phenomenon has been found in Al-Cu-Sc alloys [32]. Note that there may be more atomic columns appear to be bright Sc-containing columns at the interfaces than in reality, due to electron channelling between the columns [48].

To understand the observed Sc substitution, DFT calculations of the formation enthalpies of β′ and B′ structures with different atomic sites replaced by Sc were performed, and the results are shown in Fig. 7(a) and b, respectively. Apparently, for β′ or B′, the Mg (/Al) sites are favorable substitution sites for Sc over the Si sites, which is consistent with the experimental results. Worth mentioning is that when the Mg site of β′ is replaced by Sc, the formation enthalpy is somewhat increased (Fig. 7a), indicating that β′ with the Mg site replaced by Sc may occur in actual case, as has been demonstrated in Fig. 5c, but the Sc-free β′ phase should be more favorable. This is the reason why Sc occupation is not frequently observed in the pure β′ precipitates (Fig. 6). In addition, when the vacancy+Si site of B′ (situated at the center of sub-B′) is replaced by Sc, the formation enthalpy is significantly increased (Fig. 7b), indicating that the Sc substitution at the vacancy+Si site is unfavorable. The occasionally observed Sc substitution at the central site of sub-B′ at the precipitate interfaces is speculated to be associated with the interfacial mismatch.

Having revealed the atomic-structures of the precipitates in the Sc-containing alloy, we may now better understand the Sc-induced changes in alloy age-hardening response. Firstly, Sc addition changes the precipitates at peak-aging from well-ordered β″ to disordered β″ plus a small amount of β′. The disordered β″ is considered to be as effective as the well-ordered β″ while the β′ is much less effective in hardening the alloy. Moreover, previous studies [31,49] have demonstrated that coarse L12 Al3Sc and the V-phase with negligible strengthening contribution will form during solutionizing. The formation of these phases will consume some of the Si atoms [50] and hence decrease the volume fraction or number density of the strengthening phases formed during subsequent aging. For the above reasons, the Sc-containing alloy has a slightly lower peak-aged hardness than the Sc-free alloy. Secondly, Sc addition changes the main precipitates at the long-time over-aging from coarse β′ to relatively fine β″-related composite precipitates. The contribution to precipitation hardening from the latter must be much greater than that from the former, which explains why the Sc-containing alloy has obviously higher hardness than the Sc-free alloy after the long-

time over-aging, i. e., the Sc-containing alloy possesses better thermal stability (Fig. 2).

3.4. The Sc-tuned precipitation scenario in the Sc-containing alloy

The detailed characterization of the precipitates in the Sc-containing alloy has shown strong coupling between solute Sc and the hardening precipitates of Al-Mg-Si alloys. Next, based on the established knowledge of aging precipitation of Al-Mg-Si alloys and the atomic-structures of the composite precipitates in the Sc-containing alloy, we make a detailed discussion about the precipitation evolution in the Sc-containing alloy.

During the early stage of aging, atomic clusters of different Mg/Si ratios firstly form in the Al-matrix [51]. Here, by their Mg/Si ratio, the atomic clusters are simply classified into Si-rich (Mg/Si ratio < 1) clusters and Mg-rich (Mg/Si ratio > 1) clusters. The solute Sc could be involved in the clustering process, resulting in both types of clusters containing Sc atoms (Fig. 8a). As the binding energy of Sc-Si is much higher than that of Sc-Mg [39], Sc participation in the clustering could increase the Si/Mg atomic ratios of the clusters, and could make the Si-rich clusters richer in Sc than the Mg-rich clusters. The former means that under a certain aging time, more Si atoms could be consumed by clusters in the Sc-containing alloy. Subsequently, the Si-rich β″ precipitates nucleate on some of the Si- and Sc-rich clusters (Fig. 8b) due to the following two facts. Firstly, the nucleation energy barrier of β″ is lower than that of β′ under the relatively high solute Si concentration in the matrix [16]. Secondly, the clusters compositionally similar with the β″ phase are regarded as favorable nucleation sites for β″ [52]. However, Sc-containing disordered region universally appears in the β″ precipitates formed in the Sc-containing alloy, as can been easily deduced from the atomic-scale observation of the peak-aged Sc-containing sample where a minor fraction of ordered structure has begun to appear in the disordered regions (Fig. 5a and b). The formation of the disordered regions is interesting to understand and is inferred to be related to the following facts or reasons: Sc atoms are not able to enter the β″-structure, as has been indicated in Fig. 5(a) and (b) that there are no Sc atoms in the LDCs. In addition, there is a strong binding between Sc and Si atoms [39]. With prolonged aging time up to the peak-aging state, on the one hand, growth of the disordered β″ precipitates gradually consumes Mg and Si atoms in the matrix and, on the other hand, a large fraction of the atomic clusters remain
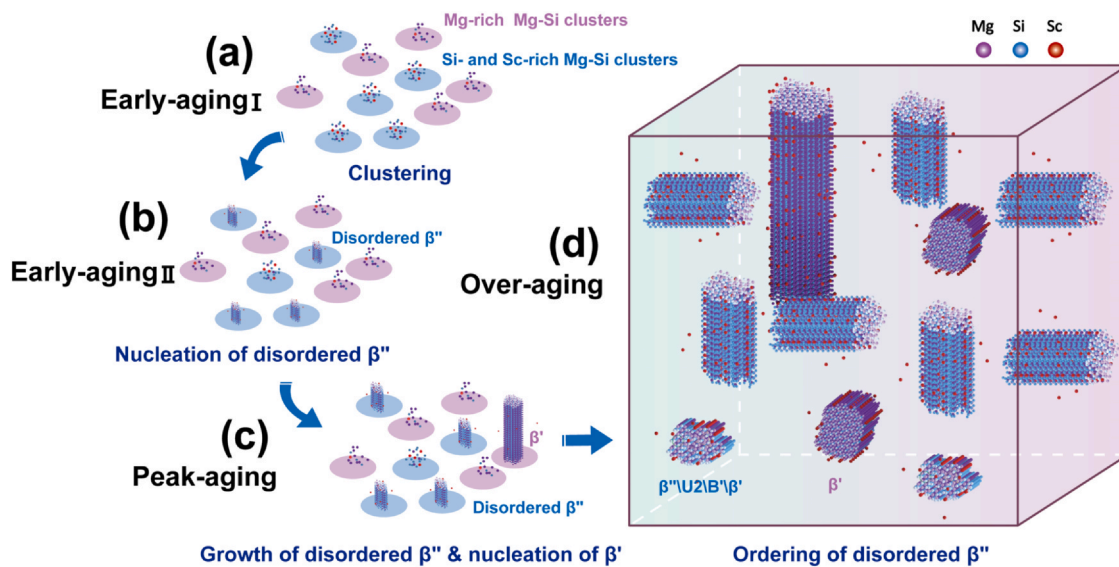
Fig. 8. Schematics showing the evolution scenarios of the precipitates in the Sc-containing Al-Mg-Si alloy upon aging. (a) Early-aging I, (b) early-aging II, (c) peak-aging, (d) over-aging.

stable. Then there exists a moment when the concentration of solute Si in the matrix decreases to the value where the nucleation energy barrier of β' is lower than that of β" [16]. At this point, nucleation of Mg-rich β' precipitates on some Mg-rich clusters occurs (Fig. 8c). Unlike the β" precipitates, the β' precipitates in the Sc-containing alloy are always well-ordered, which is probably because Sc atoms are capable of entering the β'-structure (Fig. 7a). In the investigated Sc-free alloy, the β' precipitates form at the over-aging stage (Fig. 3d), while they appear at the peak-aging or even early-aging stage in the Sc-containing alloy. This phenomenon could be because, as mentioned earlier, the Si solute atoms in the matrix are consumed more rapidly during early-aging in the Sc-containing alloy. According, it is expected that if the Si content of the Sc-containing alloy increases, the β' precipitates will form at later aging stage. It should be pointed out that the number of β' precipitates formed in the early-aged Sc-containing alloy is limited, as has been demonstrated in our results, which could be attributed to the inhibition of β' nucleation caused by prior formation of a large number of disordered β" precipitates.

Upon over-aging, two precipitation processes occur first. One is ordering of the disordered β" precipitates. The second one is growth of the β' precipitates. Through the former process, the disordered regions of the disordered β" precipitates gradually evolve to the sub-units of β'/B′/U2 while the LDCs change little, leading to formation of β"/β'/B′/U2 composite precipitates (Fig. 8d). Similar to the nucleation of β' at earlier aging stage, the formation of β'/B′/U2 sub-units at the disordered regions is also associated with the low solute Si concentration in the matrix. In the Sc-free alloy, the well-ordered β" precipitates are formed at the early-aging stage. Upon over-aging, these well-ordered β" precipitates coarsen rapidly until they are energetically unstable, and then the precipitation of the β' phase occurs gradually and eventually becomes dominating. While in the Sc-containing alloy, the sluggish ordering and transformation of the disordered β" precipitates to the β"/β'/B′/U2 composite precipitates occurs first during the over-aging period until the long-time over-aging. Our results reveal that the formation of β"-related composite precipitates is responsible for the improvement of thermal stability

of the Sc-containing alloy. Moreover, the key to the formation of these composite precipitates lies in the Sc-induced formation of the disordered β" precipitates at the early-aging stage.

4. Conclusions

In the present work, the precipitates formed in a Mg-excess Al-Mg-Si-Sc alloy aged at 180 °C have been investigated in detail by atomic-resolution HAADF-STEM. From the results presented above, the following can be concluded: The micro-alloying element Sc significantly alters the precipitate microstructures and consequently the age-hardening response of the Al-Mg-Si alloy. At the peak-aging condition, except for a small portion of β', most of the precipitates are disordered β" precipitates consisting of Sc-free β" sub-units and Sc-containing disordered regions, resulting in a slightly decreased peak hardness of the Sc-added alloy, as compared with the Sc-free alloy. During the over-aging period, the disordered regions of the disordered β" precipitates gradually evolve to the β'/B′/U2 sub-units, leading to formation of β"/β'/B′/U2 composite precipitates at the long-time over-aging. This study has revealed the microstructural origin of improved thermal stability of the Sc-added alloy. The formation of the composite precipitates is probably related to the strong binding between Sc and Si atoms, and to the non-preference for Sc atoms to occupy the atomic sites of the β"-structure. HAADF-STEM imaging along with first-principles calculations indicates that Sc partially occupy some energetically favorable atomic sites of the β' and B′ structures.

CRediT authorship contribution statement

Y. Liu: Conceptualization, Investigation, Data curation, Validation, Visualization, Writing - original draft. **Y. X. Lai:** Conceptualization, Validation, Writing - review & editing. **Z.Q. Chen:** Investigation. **S.L. Chen:** Investigation. **P. Gao:** Investigation. **J. H. Chen:** Resources, Writing - review & editing, Supervision.

Declaration of Competing Interest

The authors declare that they have no known competing financial interests or personal relationships that could have appeared to influence the work reported in this paper.

Acknowledgements

References

[1] S. Pogatscher, H. Antrekowitsch, H. Leitner, T. Ebner, P.J. Uggowitzer, Mechanisms controlling the artificial aging of Al-Mg-Si Alloys, Acta Mater. 59 (2011) 3352–3363.

[2] G.A. Edwards, K. Stiller, G.L. Dunlop, M.J. Couper, The precipitation sequence in Al-Mg-Si alloys, Acta Mater. 46 (1998) 3893–3904.

[3] J.H. Chen, E. Costan, M.A. van Huis, H.W. Zandbergen, Atomic pillar-based nanoprecipitates strengthen AlMgSi alloys, Science 312 (2006) 416–419.

[4] H.W. Zandbergen, Structure determination of Mg_5Si_6 particles in Al by dynamic electron diffraction studies, Science 277 (1997) 1221–1225.

[5] S.J. Andersen, H.W. Zandbergen, J. Jansen, C. Traeholt, U. Tundal, O. Reiso, The crystal structure of the β″ phase in Al-Mg-Si alloys, Acta Mater. 46 (1998) 3283–3298.

[6] P.H. Ninive, A. Strandlie, S. Gulbrandsen-Dahl, W. Lefebvre, C.D. Marioara, S.J. Andersen, J. Friis, R. Holmestad, O.M. Løvvik, Detailed atomistic insight into the β″ phase in Al-Mg-Si alloys, Acta Mater. 69 (2014) 126–134.

[7] H.S. Hasting, A.G. Frøseth, S.J. Andersen, R. Vissers, J.C. Walmsley, C.D. Marioara, F. Danoix, W. Lefebvre, R. Holmestad, Composition of β″ precipitates in Al-Mg-Si alloys by atom probe tomography and first principles calculations, J. Appl. Phys. 106 (2009) 123527.

[8] P.H. Ninive, A. Strandlie, S. Gulbrandsen-Dahl, W. Lefebvre, C.D. Marioara, S.J. Andersen, J. Friis, R. Holmestad, O.M. Løvvik, Detailed atomistic insight into the β″ phase in Al-Mg-Si alloys, Acta Mater. 69 (2014) 126–134.

[9] R. Vissers, M.A. van Huis, J. Jansen, H.W. Zandbergen, C.D. Marioara, S.J. Andersen, The crystal structure of the β′ phase in Al-Mg-Si alloys, Acta Mater. 55 (2007) 3815–3823.

[10] K. Matsuda, Y. Sakaguchi, Y. Miyata, Precipitation sequence of various kinds of metastable phases in Al-1.0mass% Mg_2Si-0.4mass% Si alloy, J. Mater. Sci. 35 (2000) 179–189.

[11] A.G. Frøseth, R. Høier, P.M. Derlet, S.J. Andersen, C.D. Marioara, Bonding in MgSi and Al-Mg-Si compounds relevant to Al-Mg-Si alloys, Phys. Rev. B 67 (2003) 224106.

[12] S.J. Andersen, C.D. Marioara, A. Frøseth, R. Vissers, The structural relation between precipitates in Al-Mg-Si alloys, the Al-matrix and diamond silicon, with emphasis on the trigonal phase $U1-MgAl_2Si_2$, Mater. Sci. Eng. A 444 (2007) 157–169.

[13] S.J. Andersen, C.D. Marioara, A. Frøseth, R. Vissers, H.W. Zandbergen, Crystal structure of the orthorhombic $U2-Al_4Mg_4Si_4$ precipitate in the Al-Mg-Si alloy system and its relation to the β′ and β″ phases, Mater. Sci. Eng. A 390 (2005) 127–138.

[14] H. Chen, J. Lu, Y. Kong, K. Li, T. Yang, A. Meingast, M. Yang, Q. Lu, Y. Du, Atomic scale investigation of the crystal structure and interfaces of the B′ precipitate in Al-Mg-Si alloys, Acta Mater. 185 (2020) 193–203.

[15] M.A. van Huis, J.H. Chen, H.W. Zandbergen, M.H.F. Sluiter, Phase stability and structural relations of nanometer-sized, matrix-embedded precipitate phases in Al-Mg-Si alloys in the late stages of evolution, Acta Mater. 54 (2006) 2945–2955.

[16] Y.X. Lai, B.C. Jiang, C.H. Liu, Z.K. Chen, C.L. Wu, J.H. Chen, Low-alloy-correlated reversal of the precipitation sequence in Al-Mg-Si alloys, J. Alloy. Compd. 701 (2017) 94–98.

[17] Y.X. Lai, W. Fan, M.J. Yin, C.L. Wu, J.H. Chen, Structures and formation mechanisms of dislocation-induced precipitates in relation to the age-hardening responses of Al-Mg-Si alloys, J. Mater. Sci. Technol. 41 (2020) 127–138.

[18] C.H. Liu, Y.X. Lai, J.H. Chen, G.H. Tao, L.M. Liu, P.P. Ma, C.L. Wu, Natural-aging-induced reversal of the precipitation pathways in an Al-Mg-Si alloy, Scr. Mater. 115 (2016) 150–154.

[19] N.N. Jiao, Y.X. Lai, S.L. Chen, P. Gao, J.H. Chen, Atomic-scale roles of Zn element in age-hardened AlMgSiZn alloys, J. Mater. Sci. Technol. 70 (2021) 105–112.

[20] F. Qian, D.D. Zhao, E.A. Mørtsell, S.B. Jin, J.S. Wang, C.D. Marioara, S.J. Andersen, G. Sha, Y.J. Li, Enhanced nucleation and precipitation hardening in Al-Mg-Si(-Cu) alloys with minor Cd additions, Mater. Sci. Eng.: A 792 (2020) 139698.

[21] E.A. Mørtsell, S.J. Andersen, J. Friis, C.D. Marioara, R. Holmestad, Atomistic details of precipitates in lean Al-Mg-Si alloys with trace additions of Ag and Ge studied by HAADF-STEM and DFT, Philos. Mag. 97 (2017) 851–866.

[22] T. Saito, E.A. Mørtsell, S. Wenner, C.D. Marioara, S.J. Andersen, J. Friis, K. Matsuda, R. Holmestad, Atomic structures of precipitates in Al-Mg-Si alloys with small additions of other elements, Adv. Eng. Mater. 20 (2018) 1800125.

[23] S. Wenner, L. Jones, C.D. Marioara, R. Holmestad, Atomic-resolution chemical mapping of ordered precipitates in Al alloys using energy-dispersive X-ray spectroscopy, Micron 96 (2017) 103–111.

[24] D. Shin, A. Shyam, S. Lee, Y. Yamamoto, J.A. Haynes, Solute segregation at the Al/θ′-Al_2Cu interface in Al-Cu alloys, Acta Mater. 141 (2017) 327–340.

[25] K.E. Knipling, D.C. Dunand, D.N. Seidman, Criteria for developing castable, creep-resistant aluminum-based alloys-a review, Z. Für Met 97 (3) (2006) 246–265.

[26] V.V. Zakharov, Effect of scandium on the structure and properties of aluminum alloys, Met. Sci. Heat Treat. 45 (2003) 246–253.

[27] E.P. Kwon, K.D. Woo, S.H. Kim, D.S. Kang, K.J. Lee, J.Y. Jeon, The effect of an addition of Sc and Zr on the precipitation behavior of AA6061 alloy, Met. Mater. Int. 16 (5) (2010) 701–707.

[28] Y.C. Tzeng, C.Y. Chung, H.C. Chien, Effects of trace amounts of Zr and Sc on the recrystallization behavior and mechanical properties of Al-4.5Zn-1.6Mg alloys, Mater. Lett. 228 (2018) 270–272.

[29] E.A. Marquis, D.N. Seidman, M. Asta, C. Woodward, Composition evolution of nanoscale Al_3Sc precipitates in an Al-Mg-Sc alloy: experiments and computations, Acta Mater. 54 (2006) 119–130.

[30] S.S. Yu, R.C. Wang, C.Q. Peng, Z.Y. Cai, X. Wu, Y. Feng, X.F. Wang, Effect of minor scandium addition on the microstructure and properties of Al-50Si alloys for electronic packaging, J. Mater. Sci. Mater. Electron. 30 (2019) 20070–20077.

[31] J. Røyset, N. Ryum, Scandium in aluminium alloys, Int. Mater. Rev. 50 (2005) 19–44.

[32] B.A. Chen, G. Liu, R.H. Wang, J.Y. Zhang, L. Jiang, J.J. Song, J. Sun, Effect of interfacial solute segregation on ductile fracture of Al-Cu-Sc alloys, Acta Mater. 61 (2013) 1676–1690.

[33] S. Bai, X.L. Yi, G.H. Liu, Z.Y. Liu, J. Wang, J.G. Zhao, Effect of Sc addition on the microstructures and age-hardening behavior of an Al-Cu-Mg-Ag alloy, Mater. Sci. Eng. A 756 (2019) 258–267.

[34] T. Dorina, M. Ramajayam, S. Babaniaris, L. Jiang, T.J. Langan, Precipitation sequence in Al-Mg-Si-Sc-Zr alloys during isochronal aging, Materialia 8 (2019) 100437.

[35] L. Lityńska-Dobrzyńska, Precipitation of phases in Al-Mg-Si-Cu alloy with Sc and Zr additions during heat treatment, Arch. Metall. Mater. 51 (4) (2006) 555–560.

[36] M. Vlach, J. Čížek, B. Smola, O. Melikhova, M. Vlček, V. Kodetová, H. Kudrnová, P. Hruška, Effect of Scandium addition on aging behavior of 6061 aluminum alloy, Mater. Charact. 129 (2017) 1–8.

[37] T. Nakamura, T. Matsuo, M. Ikeda, S. Komatsu, Effect of Scandium addition on aging behavior of 6061 aluminum alloy, Adv. Mater. Res. 15 (2007) 7–12.

[38] S.Y. Jiang, R.H. Wang, Grain size-dependent Mg/Si ratio effect on the microstructure and mechanical/electrical properties of Al-Mg-Si-Sc alloys, J. Mater. Sci. Technol. 35 (2019) 1354–1363.

[39] J. Peng, S. Bahl, A. Shyam, J.A. Haynes, D. Shin, Solute-vacancy clustering in aluminum, Acta Mater. 196 (2020) 747–758.

[40] P. Hohenberg, W. Kohn, Inhomogeneous electron gas, Phys. Rev. B 136 (1964) 864–871.

[41] W. Kohn, L.J. Sham, Self-consistent equations including exchange and correlation effects, Phys. Rev. A 140 (1965) 1133–1138.

[42] G. Kresse, J. Hafner, Ab initio molecular dynamics for liquid metals, Phys. Rev. B 47 (1993) 558–561.

[43] G. Kresse, J. Furthmller, Efficient iterative schemes for ab initio total-energy calculations using a plane-wave basis set, Phys. Rev. B 54 (1996) 11169–11186.

[44] G. Kresse, D. Joubert, From ultrasoft pseudopotentials to the projector augmented-wave method, Phys. Rev. B 59 (1999) 1758–1775.

[45] P.E. Blochl, Projector augmented-wave method, Phys. Rev. B 50 (1994) 17953–17979.

[46] J.P. Perdew, K. Burke, M. Ernzerhof, Generalized gradient approximation made simple, Phys. Rev. Lett. 77 (1996) 3865–3868.

[47] P.D. Nellist, S.J. Pennycook, The principles and interpretation of annular dark-field Z-contrast imaging, Adv. Imag. Electron Phys. 113 (2000) 148–203.

[48] P.D. Nellist, S.J. Pennycook, Incoherent imaging using dynamically scattered coherent electrons, Ultramicroscopy 78 (1999) 111–124.

[49] L. Lityńska-Dobrzyńska, The microstructure evolution during ageing of Al-Mg-Si alloy modified with Scandium, Appl. Crystallogr. (2004) 242–245.

[50] G. Du, J.W. Deng, Y.L. Wang, D.S. Yan, L.J. Rong, Precipitation of $(Al,Si)_3Sc$ in an Al-Sc-Si alloy, Scr. Mater. 61 (5) (2009) 532–535.

[51] M.W. Zandbergen, Q. Xu, A. Cerezo, G.D.W. Smith, Study of precipitation in Al-Mg-Si alloys by Atom Probe Tomography I. Microstructural changes as a function of ageing temperature, Acta Mater. 101 (2015) 136–148.

[52] A. Serizawa, S. Hirosawa, T. Sato, Three-dimensional atom probe characterization of nanoclusters responsible for multistep aging behavior of an Al-Mg-Si Alloy, Metall. Mater. Trans. A 39 (2008) 243–251.